

Cavity Control of Topological Qubits: Fusion Rule, Anyon Braiding and Majorana-Schrödinger Cat States

Luis Quiroga^{1,*}, Fernando J. Gómez-Ruiz², Ivan A. Bocanegra-Garay², Ferney J. Rodríguez¹, and Carlos Tejedor^{3,4}

¹*Departamento de Física, Universidad de los Andes, A.A. 4976, Bogotá D.C, Colombia*

²*Departamento de Física Teórica, Atómica y Óptica, Universidad de Valladolid, 47011 Valladolid, Spain*

³*Departamento de Física Teórica de la Materia Condensada,
Universidad Autónoma de Madrid, Madrid 28049, Spain*

⁴*Condensed Matter Physics Center (IFIMAC), Universidad Autónoma de Madrid, Madrid 28049, Spain*

We investigate the impact of introducing a local cavity within the center of a topological chain, revealing profound effects on the system's quantum states. Notably, the cavity induces a scissor-like effect that bisects the chain, liberating Majorana zero modes (MZMs) within the bulk. Our results demonstrate that this setup enables the observation of non-trivial fusion rules and braiding—key signatures of non-Abelian anyons—facilitated by the spatially selective ultra-strong coupling of the cavity photon field. These MZM characteristics can be directly probed through fermionic parity readouts and photon Berry phases, respectively. Furthermore, by leveraging the symmetry properties of fermion modes within a two-site cavity, we propose a novel method for generating MZM-polariton Schrödinger cat states. Our findings present a significant advancement in the control of topological quantum systems, offering new avenues for both fundamental research and potential quantum computing applications.

Introduction.— Topological quantum computing is a holy grail of current research on quantum technologies [1]. Its key building blocks are non-abelian anyon quasi-particles in topological matter [2–4]. Clear experimental evidence on such anyons is still missing but recent advances in precision control of hybrid semiconductor-superconductor nanowires and quantum dot arrays have brought researchers closer to their realization [5, 6]. This opens new possibilities in designing novel experimental frameworks while making conceptual questions of great relevance.

The essential physics of 1D Ising anyons is captured by the Kitaev chain (KC) model [7]. Each local Dirac fermion of the chain can be expressed in terms of a pair of Majorana fermions (MF). A key consequence is the existence of a topological phase in which a zero energy mode exists. It consists of two MF each one localized at one edge of the chain. Occupied and unoccupied options of such state have zero energy, forming a non-local qubit. Due to the splitting of the Majorana zero mode (MZM), quantum information is stored in both halves (data redundancy). If one half of the mode suffers interference, there is still enough information stored in the other half to proceed with the computation. Moreover, MZM become decoupled from the rest of the KC being an excellent candidate to present non-abelian statistics. Topological protection is produced through braiding and measurement of the non-abelian anyon character of MZM.

Recently, braiding and quantum teleportation of delocalized Majorana qubits have been established in KC manipulated by superconducting resonators [8, 9]. This remarkable experimental achievement prompts us to elaborate on extended scenarios to theoretically investigate for further non-local features in condensed matter systems aiming to put on firm grounds topological quantum computation routines. The most popular scheme proposed to achieve anyon braiding in topological 1D wire networks relies on a T-junction geometry [10–12]. The goal of most studies has been to explore how

the pairing between different MF featuring an MZM evolves under a cyclic tuning of different coupling schemes. These simulations can be challenging both experimentally and theoretically. On the other side, the question of what might happen with an anyon fusion or braiding protocol relying on a purely geometric quantum state property has received far less attention.

The present work aims to pave the way to an alternative to multi-wire T-junction schemes: the analysis of the potential capabilities of a wire topological network controlled by the coupling to a bosonic environment in the regime of cavity quantum electrodynamics. This would open the use of photons and topological matter-connected states for new strategies to harness non-classical aspects of both matter and radiation ranging from fundamental physics aspects to potential applications in quantum information/computation issues. This becomes even more relevant in powerful platforms with novel quantum materials strongly coupled to optical and microwave cavities [13–18] where photon quantum states, specifically coherent and squeezed states, show great promise in this regard due to the ease of availability and well-established control techniques.

In stark contrast to previous proposals that aimed the demonstration of Majorana fusion rule using diverse connecting elements (quantum dots or electrostatic gates), to mediate the exchange between different KC edge MZMs [11, 12, 19, 20], our proposed KC-cavity set up is based on a *single* KC in the deep topological phase. In this way, the cavity acts as a scissor, splitting the original KC into two halves and consequently generating two new MZMs (for a fully electrostatic cutting way see [21]). The basic idea of previous works with cavity-controlled MZM systems [22–24] was primarily focused on the lowest-order photon-MZM coupling effects, i.e. where pre-defined MZM already existed before embedding the topological matter within the cavity, instead of a genuine full polariton image. Here, we propose a signifi-

cantly distinct physics framework: the local cavity acts as a topological scissor [25], giving rise to a set of MZMs at the ends of the two parts of the original KC outside the cavity. Furthermore, it enables the simulation of their exchange by gathering up the precise Berry phase of the cavity field under an adiabatic cyclic variation of the matter-light coupling strength. As we will demonstrate below, for low and intermediate coupling strengths the polariton state is an entangled matter-light state. Nevertheless, in the ultra-strong coupling (USC) regime, the asymptotic decoupling of light and matter degrees of freedom [26, 27] enables both anyon fusing and braiding processes, mediated by photons, to occur in a KC-cavity system. Moreover, highly non-classical photon states in the cavity, Schrödinger cat states assisted by Majorana non-local qubits, become accessible. Such features turn out to be within reach in the USC regime due to the burgeoning interest on new cavity quantum electrodynamics (cQED) architectures and material supports [14–16]. The USC is particularly interesting for going beyond such first-order effects. The transition between different photon coherent states goes with corresponding modifications of fermion correlations. Moreover, of particular interest is the fact that in the asymptotic decoupling regime, cavity decoherence effects turn out to be innocuous for the MZM dynamics.

Model system.— We consider a single KC with vanishing chemical potential $\mu = 0$, and identical hopping (t) and pairing (Δ) terms, i.e. $t = \Delta$, the so-called sweet-spot for a quantum dot realization of the minimal KC [21]. For vanishing chemical potential the Kitaev Hamiltonian takes a diagonal form in terms of new non-local fermion operators \hat{d}_j and \hat{d}_j^\dagger , i.e. $\hat{H}_{\text{KC}} = 2\Delta \sum_{j=1}^{N-1} \left[\hat{d}_j^\dagger \hat{d}_j - \frac{1}{2} \right] = i\Delta \sum_{j=1}^{N-1} \hat{\gamma}_{j,2} \hat{\gamma}_{j+1,1}$ (see Supplemental Material (SM) [28] and Ref. [29] for their definition in terms of both original Kitaev local operators ($\hat{c}_j^\dagger, \hat{c}_j$) or Majorana fermions ($\hat{\gamma}_{j,1}, \hat{\gamma}_{j,2}$)). The single mode microcavity Hamiltonian takes the usual form $\hat{H}_C = \omega \hat{a}^\dagger \hat{a}$, where ω is the photon quantum energy ($\hbar = 1$). Finally, the KC-cavity coupling term is given by $\hat{H}_X = \frac{1}{\sqrt{n_{\text{Cav}}}} \sum_{j \in \text{Cav}} \lambda_j \hat{c}_j^\dagger \hat{c}_j (e^{-i\phi_j} \hat{a}^\dagger + \hat{a} e^{i\phi_j})$ with λ_j the coupling strength between the KC j -site and the cavity field, Cav is the set with the site indices interacting with the cavity and ϕ_j controllable phases [30].

The simplest case corresponds to a cavity coupled to a single bulk site at $j = s$, from now on labeled as 1CK case as depicted in Fig.1(a). The coupling term \hat{H}_X Hamiltonian involves the number operator $\hat{c}_s^\dagger \hat{c}_s = \frac{1}{2} (1 + \hat{d}_{s-1} \hat{d}_s + \hat{d}_{s-1} \hat{d}_s^\dagger - \hat{d}_{s-1}^\dagger \hat{d}_s - \hat{d}_{s-1}^\dagger \hat{d}_s^\dagger)$. Since only two d -fermion operators (\hat{d}_{s-1} and \hat{d}_s) are included in the matter-radiation coupling, just 4 matter states are involved in the full system quantum evolution. Moreover, without loss of generality, we consider only the reduced subspace of even fermion parity (dimension 2), spanned by the eigenstates of the $\hat{\sigma}_z$ Pauli operator, $\hat{\sigma}_z |\pm\rangle_z = \pm |\pm\rangle_z$, i.e. the basis states are chosen as $|-\rangle_z = |\circ\circ\rangle$ and $|+\rangle_z = \hat{d}_{s-1}^\dagger \hat{d}_s^\dagger |\circ\circ\rangle = |\bullet\bullet\rangle$, where $|\circ\circ\rangle$ represents the vacuum state, i.e., no d -fermion excitations, or

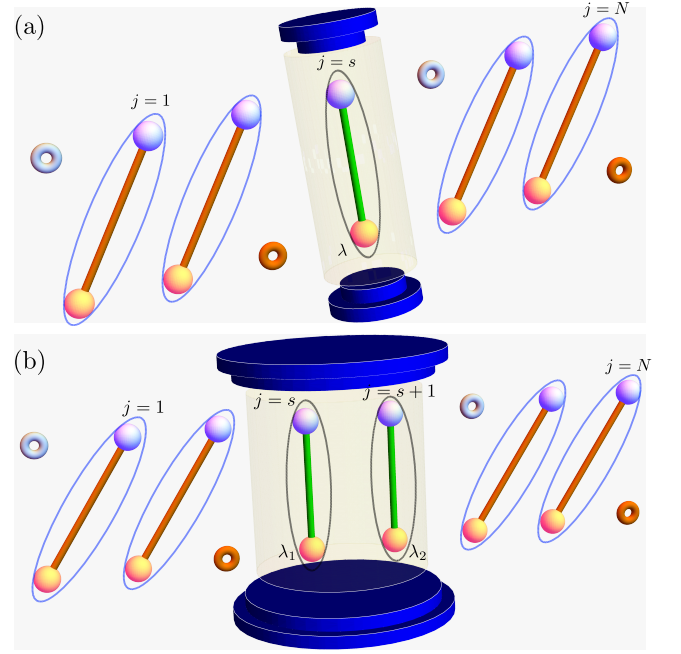


FIG. 1. Schematic representation of Kitaev chain-cavity systems. In the topological phase, a Kitaev chain is schematically represented by colored balls and links. The balls represent Majorana fermions $\gamma_{j+1,1}$ and $\gamma_{j,2}$ with different colors, indicating the localization of a free MZM as a torus. The cavity is depicted by two blue mirrors, operating as natural topological scissors. The KC-cavity interaction in the USC regime allows the formation of local Dirac fermions located inside the cavity. (a) corresponds to the 1CK case while (b) depicts the 2CK case. The radiation-matter interaction is represented by λ_r , with $r = 1, 2$.

$\hat{d}_j |\circ\circ\rangle = 0$ for $j = s-1, s$. Consequently, the 1CK Hamiltonian reduces to that of an effective Rabi-like model with homodyne rotated quadrature:

$$\hat{H}_1 = -2\Delta \hat{\sigma}_z + \omega \hat{a}^\dagger \hat{a} + \frac{\lambda}{2} (e^{-i\phi} \hat{a}^\dagger + e^{i\phi} \hat{a}) (1 - \hat{\sigma}_x). \quad (1)$$

Similarly, for a cavity enclosing two contiguous KC sites (from now on 2CK case, Fig. 1(b), sites $j = s$ and $j = s+1$, or equivalently only three d -fermion operators (\hat{d}_{s-1}, \hat{d}_s and \hat{d}_{s+1}) are brought into play so just 4 matter states are involved in the full system quantum evolution, a two-qubit effective Rabi-like Hamiltonian arises:

$$\hat{H}_2 = -\Delta (\hat{\sigma}_{z,1} + \hat{\sigma}_{z,2} + \hat{\sigma}_{z,1} \hat{\sigma}_{z,2}) + \omega \hat{a}^\dagger \hat{a} + \frac{1}{2\sqrt{2}} \sum_{r=1}^2 \lambda_r (e^{-i\phi_r} \hat{a}^\dagger + e^{i\phi_r} \hat{a}) (1 - \hat{\sigma}_{x,r}), \quad (2)$$

where $\hat{\sigma}_{v,r}$, with $v = x, y, z$, denote Pauli matrices for spin $r = 1, 2$, complex valued $\lambda_1 e^{-i\phi_1}$ and $\lambda_2 e^{-i\phi_2}$ represent the coupling strengths at sites s and $s+1$, respectively (see SM [28]). Restriction to the even fermion parity sector has been kept.

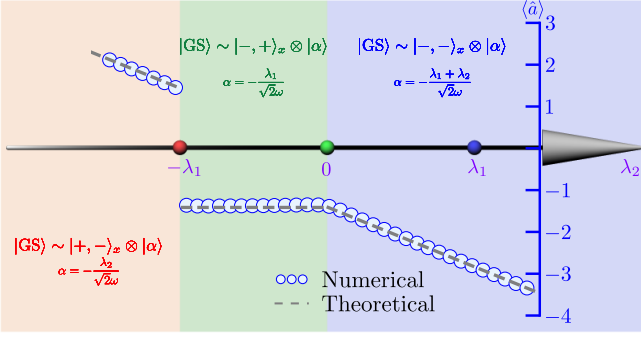


FIG. 2. **2CK ground state phase diagram in the USC regime.** Inhomogeneous system, i.e. real valued $\lambda_2 \neq \lambda_1$. Full numerical (open circles) and USC theoretical results (broken line) for the photonic coherent state displacement $\langle \hat{a} \rangle$ are put on top: $\lambda_1/2\Delta = 4$ and resonance condition $\omega/2\Delta = 2$. See main text for details.

Notice that for both 1CK and 2CK cases, the resonance condition between matter and photonic sub-systems is $\omega = 4\Delta$ and the d -fermion parity is a constant of motion, i.e. a single photon can only produce changes on the d -fermion occupation number by $0, \pm 2$.

In the USC regime, the 2CK ground state displays a clear decoupling between matter and photon states for any pair (λ_1, λ_2) , as shown in Fig. 2, except for the special point $\lambda_2 = -\lambda_1$ where a superposition of even and odd Schrödinger cat states occurs. Simultaneously, a sudden jump of the coherent state displacement α takes place when crossing this special point. Signatures of those transitions are also imprinted in the photon distribution (see Fig. 2), allowing for optical readout schemes. These special features will be exploited below to set up a braiding protocol.

Fusion rule.— MZMs are Ising anyons obeying the fusion rule $\sigma \times \sigma = 1 + \Psi$, where two Ising anyons (σ) fuse into either a vacuum (1) or a standard Dirac fermion (Ψ) [21, 31]. Fusion rule experiments are in general simpler than braiding experiments, thus they are first-ever candidates for testing the non-Abelian features of MZMs.

In the present cavity setup, for testing the non-trivial fusion rule only a pair of MZMs is required. We consider the fusion rule in the 1CK case by adiabatically increasing the KC-cavity coupling strength. Thus, we start with a single uncoupled KC in its ground state featuring a pair of MZMs located at the chain edges. During the whole process, the total fermionic parity of the KC states is fixed to be even (+1) as we start with the ground state of a non-interacting KC-cavity, i.e. $|\chi_1\rangle = |-\rangle_x \otimes |0_{\text{ph}}\rangle$ where $|0_{\text{ph}}\rangle$ denotes the photon vacuum state. After the cavity is strongly coupled to the KC two new MZMs emerge at the neighbor sites of the cavity as previously demonstrated in Ref. [25].

One immediate consequence of the H_1 structure in Eq. (1) is the expression for its USC limit eigenstates: if $\lambda \gtrsim \omega \gg \Delta$, the matter-light eigenstates become uncoupled, given by the separable states $|\Psi\rangle \approx |-\rangle_x \otimes |\alpha\rangle$ where $\hat{\sigma}_x |-\rangle_x = -|-\rangle_x$ and the photon state is nothing but the coherent state $|\alpha\rangle$ with $\alpha =$

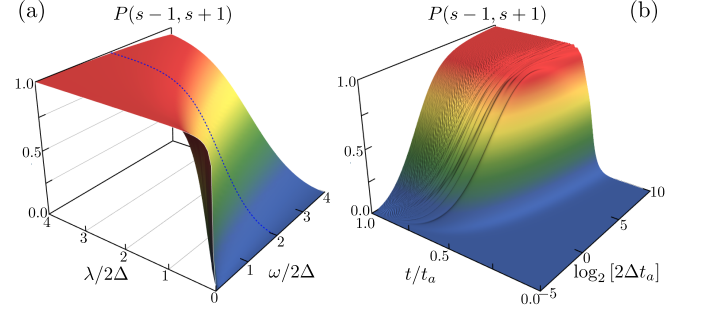


FIG. 3. **Fusion rule protocol in a 1CK system.** In panel (a), we depict the ground state fermion correlation function $P(s-1, s+1)$, with the dashed blue line representing the resonance condition. In panel (b), for the resonant case, we consider a time-dependent linear ramping of the radiation-matter interaction coupling strength, $\lambda = vt = t/t_a$ with $v = t_a^{-1}$ the ramping rate, where the evolution time $t \in [0, 4t_a]$.

$-\lambda/\omega$. Thus, the final matter state, after adiabatically turning on the KC-cavity coupling until the USC regime is reached, turns out to be $|-\rangle_x = (|\circ\circ\rangle - |\bullet\bullet\rangle)/\sqrt{2}$ indicating once more that the cavity coupling doesn't alter the total fermionic parity. Therefore, the final matter state is an equal probability superposition of states with no fermions on each side of the cavity and states with a single fermion on each side. The fusion outcome becomes probabilistic, not deterministic, as clearly indicated by the resulting KC-cavity state. This result corresponds to a positive test of the fusion protocol of two Ising anyons. In the case of quantum dot-based Kitaev systems the readout of the fusion outcome can be detected by standard capacitance measurements or tunneling signatures [32]. We numerically test the validity of the fusion protocol in 1CK system by diabatically turning on the matter-light coupling strength. For that purpose we evaluate the fermion correlation function of the two nearest neighbor Majorana fermions to the cavity, $P(s-1, s+1) = i\langle \gamma_{s-1,2}, \gamma_{s+1,1} \rangle = -\langle \hat{\sigma}_x \rangle$. Figure 3(a) shows a 3D plot of that correlation in the ground state as a function of photon energy and coupling strength ($\phi = 0$). To test for diabatic errors, we show the same correlation function in Fig. 3(b) for time-dependent cases with different velocities of turning on of the matter-photon coupling strength (different ramping rates). Notably, we obtain an excellent agreement between analytical and numerical results, even well beyond the realm of applicability of the USC regime, for sufficiently slow ramping processes.

Braiding protocol.— As a further step, we propose a cavity-chain setup to perform an MZM braiding/exchange process. Most recipes for simulations of braiding protocols in 1D topological systems rely on either Floquet dynamics (Majorana time crystals [33]) or quantum dot mediated exchange [21, 34]. The former case demands extreme timing control while the latter scheme requires a vanishing dot energy level splitting which hampers an adiabatic evolution harming the goal of a geometric phase $\pi/4$, as required for a perfect exchange

between two MZMs. Our goal is to reach the same $\pi/4$ -phase by performing an adiabatic cyclic process on the cavity itself, i.e. on the coherent state $|\alpha\rangle$, by leveraging the separable property of the ground state (GS) in the USC regime, i.e. $|\text{GS}\rangle \simeq |\chi\rangle \otimes |\alpha\rangle$ with $|\chi\rangle$ a matter KC state. In our setup, the polariton KC-cavity state can be coupled to the Majorana state, and so is not involved in braiding, only initialization (and possibly readout).

Consider a 2CK acting on chain sites $j = s$ (coupling strength $\lambda_1 e^{i\phi_1}$) and $j = s + 1$ (coupling strength $\lambda_2 e^{i\phi_2}$), governed by H_2 in Eq. (2). Let us start by fixing $\lambda_1 > 0$ in the USC regime and $\phi_1 = 0$, without any loss of generality, while λ_2 and ϕ_2 can be tunable. The MF just to the left of the cavity, i.e. $\hat{\gamma}_L = \hat{\gamma}_{s-1,2}$, always behaves as a free MZM [25] while $\hat{\gamma}_R = \hat{\gamma}_{s+1,1}$ acquires the MZM condition only in the $\lambda_2 \rightarrow 0$ regime. We will be focusing on the braiding process between these two MFs, $\hat{\gamma}_L$ and $\hat{\gamma}_R$.

For $\phi_1 = 0$, the composite ground state in the USC regime becomes

$$|\text{GS}_\pm\rangle \simeq \begin{cases} -i|\Psi_+\rangle \otimes |\alpha_+\rangle, & \text{for } \phi_2 = 0, \\ +i|\Psi_-\rangle \otimes |\alpha_-\rangle, & \text{for } \phi_2 = \pi. \end{cases} \quad (3)$$

Where $|\Psi_\pm\rangle = (|\bullet_{L,R}, \bullet_{c_1}, \circ_{s+1}\rangle \pm |\circ_{L,R}, \bullet_{c_1}, \bullet_{s+1}\rangle)/\sqrt{2}$, $\alpha_+ = -(\lambda_1 + \lambda_2)/(\sqrt{2}\omega)$, and $\alpha_- = -\lambda_1/(\sqrt{2}\omega)$ regardless the value of $\lambda_2 \leq \lambda_1$. In the 1CK limit, i.e. $\lambda_2 \rightarrow 0$, the system's ground state turns out to be

$$\begin{aligned} |\text{GS}\rangle &\simeq \frac{1}{\sqrt{2}} (|\text{GS}_+\rangle - |\text{GS}_-\rangle), \\ &= |\bullet_{L,R}, \bullet_{c_1}, \circ_{s+1}\rangle \otimes |\alpha\rangle. \end{aligned} \quad (4)$$

With $\alpha = -\lambda_1/(\sqrt{2}\omega)$. The braiding or exchange process between $\hat{\gamma}_L$ and $\hat{\gamma}_R$ MFs, as described by the operator $\hat{U}_B^{(L,R)} = e^{\frac{\pi}{4}\hat{\gamma}_L\hat{\gamma}_R} = \frac{1}{\sqrt{2}}(1 + \hat{\gamma}_L\hat{\gamma}_R)$ (performing the exchange transformations $\hat{\gamma}_L \rightarrow \hat{\gamma}_R$ and $\hat{\gamma}_R \rightarrow -\hat{\gamma}_L$), when acting on the ground state produces the result $\hat{U}_B^{(L,R)}|\text{GS}\rangle = e^{-i\frac{\pi}{4}}|\text{GS}\rangle$. By using a local phase shifter acting just on the $j = s + 1$ chain site [30, 35–37], a controlled complex coupling strength $\lambda_2 e^{i\phi_2}$ should be possible enabling a cyclic evolution of the cavity coherent state $|\alpha\rangle$ and consequently to access to a specific Berry phase of the whole matter-photon state (dynamic phases which depend on the system's specific time evolution may be experimentally canceled out [38, 39]).

Now, we focus on recovering the same $e^{-i\frac{\pi}{4}}$ global phase factor on the GS by performing an adiabatic cyclic evolution of the coherent cavity field (Berry phase). The GS adiabatic evolution is fully contained in the two-dimensional sub-space spanned by the states $\{|\text{GS}_+\rangle, |\text{GS}_-\rangle\}$, as previously assured (for details see the SM). We perform a cyclic evolution of the GS by fixing a $\lambda_2 > 0$ value while varying the phase $\phi_2 = \phi$ of the coupling strength, $0 \leq \phi \leq 2\pi$. Thus, for the GS we have $|\text{GS}(\phi)\rangle = C_+(\phi)|\text{GS}_+(\phi)\rangle + C_-(\phi)|\text{GS}_-(\phi)\rangle$. Notice that the state $|\text{GS}_-\rangle$ does not depend on the phase ϕ . We proceed with an analytical calculation of the Berry phase using the

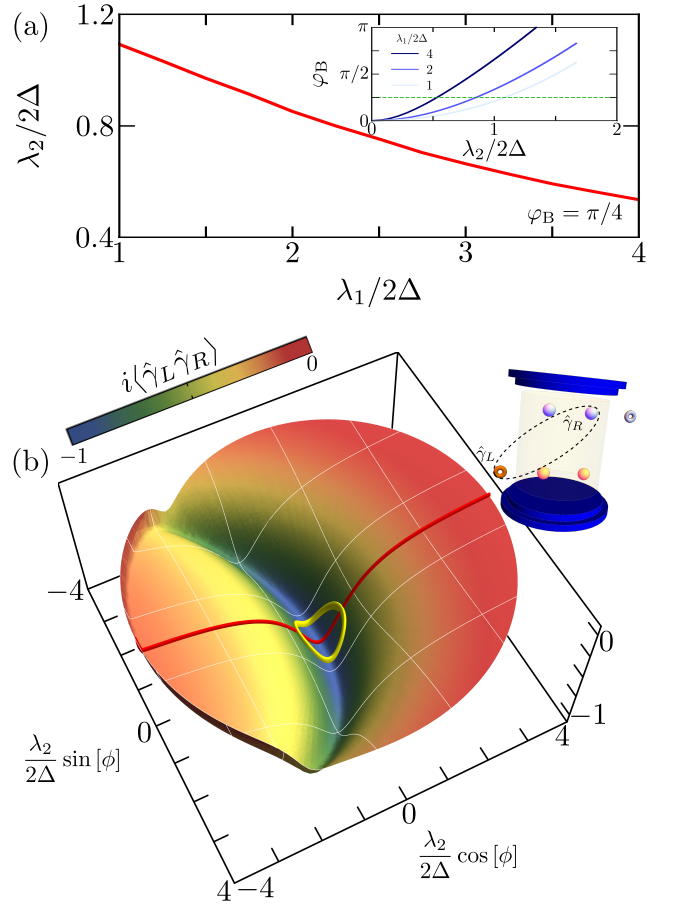


FIG. 4. **Signature of MZM Braiding in a 2KC Setup.** In panel (a), we depict the numerical relationship between the couplings λ_2 as a function of λ_1 , where the Berry phase is exactly $\pi/4$. In the inset of panel (a), we show the behavior of the Berry phase by numerical evaluation of Eq. (5) for several values of λ_1 . In panel (b), we illustrate the landscape of parity between γ_L and γ_R .

sub-space-confined evolution of the GS. By direct calculation, we obtain:

$$\varphi_B = \int_0^{2\pi} \frac{d\phi}{2\omega} \delta E_\phi \left[1 - \frac{\delta E_\phi}{\sqrt{4\Delta^2 |\langle \alpha_- | \alpha_+(\phi) \rangle|^2 - \delta E_\phi^2}} \right]. \quad (5)$$

Where, we are using $\delta E_\phi = \omega(|\alpha_+(\phi)|^2 - |\alpha_-|^2)$, $\alpha_- = -\lambda_1/(\sqrt{2}\omega)$, and $\alpha_+(\phi) = -(\lambda_1 + \lambda_2 e^{i\phi})/(\sqrt{2}\omega)$. If $\Delta \ll \lambda_2$, the Berry phase $\varphi_B \rightarrow \pi\lambda_2^2/\omega^2$, coinciding exactly with the Berry phase of a pure coherent state with $\alpha = -\lambda_2/(\sqrt{2}\omega)$ under an adiabatic cyclic evolution [40]. A numerical evaluation of Eq. (5) allows us to make a plot of λ_2 as a function of λ_1 to get a Berry phase of just $\pi/4$, as shown in Fig. 4(a). As it is evident from that figure to reach the appropriate Berry phase the coupling strength with the right KC site $\lambda_2 \ll \lambda_1$, validating the ground state structure displayed by Eq. (4). Measurement of the photon Berry phase in superconducting cavity systems has been widely discussed previously [41].

The parity $P_{L,R} = i\langle \hat{\gamma}_L \hat{\gamma}_R \rangle$, between $\hat{\gamma}_L$ and $\hat{\gamma}_R$ MFs, is plotted in Fig. 4(b) as a function of $\lambda_2 e^{i\phi_2}$, for $0 \leq \lambda_2 \leq \lambda_1$ and $0 \leq \phi_2 \leq 2\pi$. $P_{L,R} \rightarrow -1$ for $\lambda_2 \approx 0$ in agreement with the GS given by Eq. (4). The solid red line shows the corresponding results for varying real λ_2 values from the positive to the negative region. At the same time, the closed curve depicts the $P_{L,R}$ evolution just at the λ_2 value producing the correct Berry phase of $\pi/4$, simulating the perfect braiding/exchange between $\hat{\gamma}_L$ and $\hat{\gamma}_R$ MFs.

Majorana-Schrödinger cat states.— Photon Schrödinger cat states have been intensively studied in circuit quantum electrodynamics scenarios since they offer the opportunity of investigating fundamental tests of quantum theory, for encoding logical qubits and for developing error correction codes [42]. A Schrödinger cat-like state can be written as $|\mathbf{Cat}_\pm\rangle = (|\alpha\rangle \pm |-\alpha\rangle)/N_\pm$ with normalization constant $N_\pm^2 = 2(1 \pm \exp[-2|\alpha|^2])$ and sign + (−) for even (odd) cat state. Interestingly enough, in the USC regime, a 2CK system supports photon Schrödinger cat states coupled to Majorana fermion states at the special coupling values $\lambda_1 = \lambda_2 = \lambda$, $\phi_1 = 0$, and $\phi_2 = \pi$. The 2CK ground state becomes:

$$\begin{aligned} |\mathbf{GS}\rangle &\simeq |+, -\rangle_x \otimes |-\alpha\rangle + |-, +\rangle_x \otimes |\alpha\rangle, \\ &\simeq |\tilde{\Psi}_+\rangle \otimes |\mathbf{Cat}_+\rangle + |\tilde{\Psi}_-\rangle \otimes |\mathbf{Cat}_-\rangle. \end{aligned} \quad (6)$$

Where, we are using $\alpha = -\lambda/(\sqrt{2}\omega)$, $|\tilde{\Psi}_\pm\rangle = (| \bullet_{L,R}, \circ_{c_1}, \bullet_{c_2} \rangle \pm | \bullet_{L,R}, \bullet_{c_1}, \circ_{c_2} \rangle)/\sqrt{2}$, and the matter basis set $\{|n_{L,R}, n_{c_1}, n_{c_2}\rangle\}$ has been used (number occupation representation of the non-local fermion $f_{L,R}$ and two local fermions fully contained inside the cavity, c_1 and c_2 , see SM [28]). The result in Eq. (6) indicates that the system's ground state is an entangled KC-cavity state: the symmetric combination of the two local fermion (c_1, c_2) state couples with an even Schrödinger cat state whereas the anti-symmetric two fermion state couples to the odd Schrödinger cat state. Therefore, conditioned on the symmetry measurement outcome of the fermion state inside the 2CK, an even or odd cavity cat state can be distilled. In the resonant case, the ground state of the Hamiltonian given by Eq. (2) is numerically obtained through exact diagonalization from which the reduced photon density matrix immediately is within reach for the GS out of the special point $\lambda_1 = \lambda_2 = \lambda$, $\phi_1 = 0$, and $\phi_2 = \pi$. As depicted in the upper-lateral plots in Fig. 5 the Wigner functions do not display negative features as expected for coherent states. However, for the special set of coupling strengths we are considering in Eq. (6), after a previous projection of the GS on the matter states $|\tilde{\Psi}_\pm\rangle$, the corresponding Wigner function displays negative values in the central plots of Fig. 5, a fingerprint of Majorana induced Schrödinger cat states.

Importantly, the generation of Schrödinger cat states in the 2CK system is independent of the resonance condition or dispersive condition, and neither a nonlinear Kerr medium is required. Furthermore, the dissipation effect of losing one excitation results, at some random time, in an inversion of parity of the cat state, i.e. even cat states transform to odd cat states

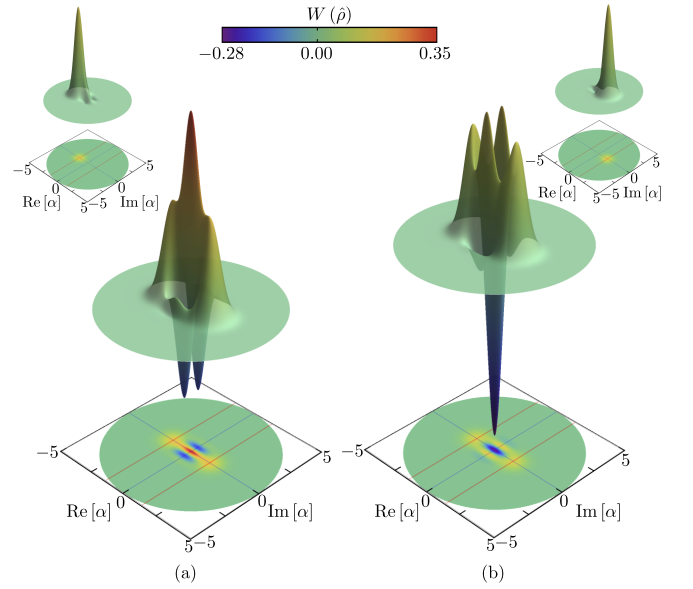


FIG. 5. **Majorana-Schrödinger cat states.** In the main panels (a) and (b), the bosonic Wigner function is represented, conditioned on the symmetry measurement outcome of the fermion state inside the 2CK in the resonance case. An even (panel (a)) or odd (panel (b)) cavity cat state is distilled. The red lines over the density projections correspond to the values of $\alpha = \pm\lambda/(\sqrt{2}\omega)$, with $\lambda = 4$ fixed. Similarly, the insets correspond to the numerical Wigner functions obtained when the ground state is projected onto $|+, -\rangle_x$ and $|-, +\rangle_x$, respectively.

(and vice versa).

Summary and discussion.— In this work, we report on a diverse range of new features of anyons that can be significant for harnessing cavity confinement control over quantum topological materials. Our results not only uncover new facets of anyon-photon composed states at a fundamental level but also have interesting applications, such as braiding-allowed teleportation schemes in the USC regime. Our findings provide useful insights into how superconducting circuit cavity control is indeed a feasible alternative to test non-Abelian anyon statistics associated with MZMs. This would provide a stringent test of the theory of free Majorana fermions in nanowire or quantum dot array scenarios.

Enhanced experimental capabilities to control superconducting quantum electrodynamics circuits are currently fuelling intense research in the domain of light-matter systems. Harnessing ultra-strong couplings is thus not only of fundamental interest but also of appeal for technological applications. Regarding the experimental feasibility of the above-discussed results, it is worth noting that the KC model has been demonstrated experimentally in a fully controlled chain of coupled quantum dots where fine-tuning of parameters lays out the system into a sweet spot which leads to the generation of poor man's Majorana states [6]. The next step should be the coupling to a transmission line resonator. With properly applied driving on the resonator mode or directly on the

KC sites embedded within the cavity, the cavity-controlled KC features can be observed from the transmission spectrum [23, 24, 36, 37], by quantum process tomography [38] or by microwave interferometric measurements [39].

An interesting prospect is to generalize these single cavity controlled anyon processes to multi-cavity setups offering tools to observe geometric phase controlled braiding mechanisms offering new paths for further exploration. Besides, dissipation is something that cannot be avoided in experiments and thus should be accounted for in studying the photon-matter correlation transitions.

Acknowledgments.— L.Q. and F.J.R. would like to thank Facultad de Ciencias-UniAndes projects: INV-2021-128-2292 and INV-2023-162-2833 for financial support. F.J.G-R and I.A.B-G acknowledge financial support from Spanish MCIN with funding from European Union Next Generation EU (PRTRC17.I1) and Consejería de Educacion from Junta de Castilla y Leon through QCAYLE project, as well as grants PID2020-113406GB-I00 MTM funded by AEI/10.13039/501100011033, and RED2022-134301-T. C.T. acknowledges financial support from the project “Nanofotonica para Computacion Cuantica” (NanoQuCo) with reference Y2020/TCS-6545 of the Comunidad de Madrid (CAM).

-
- [1] S. Das Sarma, M. Freedman, and C. Nayak, Topological quantum computation, *Phys. Tod.* **59**, 32 (2006).
- [2] C. Nayak, S. H. Simon, A. Stern, M. Freedman, and S. Das Sarma, Non-Abelian anyons and topological quantum computation, *Rev. Mod. Phys.* **80**, 1083 (2008).
- [3] A. Stern, Anyons and the quantum hall effect – A pedagogical review, *Ann. Phys.* **323**, 204–249 (2008).
- [4] C. Song, D. Xu, P. Zhang, J. Wang, Q. Guo, W. Liu, K. Xu, H. Deng, K. Huang, D. Zheng, S.-B. Zheng, H. Wang, X. Zhu, C.-Y. Lu, and J.-W. Pan, Demonstration of topological robustness of anyonic braiding statistics with a superconducting quantum circuit, *Phys. Rev. Lett.* **121**, 030502 (2018).
- [5] S. M. Albrecht, A. P. Higginbotham, M. Madsen, F. Kuemmeth, T. S. Jespersen, J. Nygard, P. Krogstrup, and C. M. Marcus, Exponential protection of zero modes in majorana islands, *Nature* **531**, 206–209 (2016).
- [6] T. Dvir, G. Wang, N. van Loo, C.-X. Liu, G. P. Mazur, A. Bordin, S. L. D. ten Haaf, J.-Y. Wang, D. van Driel, F. Zlatelli, X. Li, F. K. Malinowski, S. Gazibegovic, G. Badawy, E. P. A. M. Bakkers, M. Wimmer, and L. P. Kouwenhoven, Realization of a minimal kitaev chain in coupled quantum dots, *Nature* **614**, 445–450 (2023).
- [7] A. Y. Kitaev, Unpaired majorana fermions in quantum wires, *Phys-Usp* **44**, 131–136 (2001).
- [8] H.-L. Huang, M. Narożniak, F. Liang, Y. Zhao, A. D. Castellano, M. Gong, Y. Wu, S. Wang, J. Lin, Y. Xu, H. Deng, H. Rong, J. P. Dowling, C.-Z. Peng, T. Byrnes, X. Zhu, and J.-W. Pan, Emulating quantum teleportation of a majorana zero mode qubit, *Phys. Rev. Lett.* **126**, 090502 (2021).
- [9] H.-L. Huang, D. Wu, D. Fan, and X. Zhu, Superconducting quantum computing: a review, *Sci. China Inf. Sci.* **63**, 10.1007/s11432-020-2881-9 (2020).
- [10] J. Alicea, Y. Oreg, G. Refael, F. von Oppen, and M. P. A. Fisher, Non-abelian statistics and topological quantum information processing in 1d wire networks, *Nat. Phys.* **7**, 412–417 (2011).
- [11] D. Aasen, M. Hell, R. V. Mishmash, A. Higginbotham, J. Danon, M. Leijnse, T. S. Jespersen, J. A. Folk, C. M. Marcus, K. Flensberg, and J. Alicea, Milestones toward majorana-based quantum computing, *Phys. Rev. X* **6**, 031016 (2016).
- [12] D. J. Clarke, J. D. Sau, and S. Das Sarma, Probability and braiding statistics in majorana nanowires, *Phys. Rev. B* **95**, 155451 (2017).
- [13] F. J. Gómez-Ruiz, F. Rodríguez, L. Quiroga, and N. F. Johnson, Vulnerability of quantum information systems to collective manipulation, in *Quantum Information Science - Recent Advances and Computational Science Applications [Working Title]* (IntechOpen, 2024).
- [14] J. Bloch, A. Cavalleri, V. Galitski, M. Hafezi, and A. Rubio, Strongly correlated electron–photon systems, *Nature* **606**, 41–48 (2022).
- [15] F. J. García-Vidal, C. Ciuti, and T. W. Ebbesen, Manipulating matter by strong coupling to vacuum fields, *Science* **373**, 10.1126/science.abd0336 (2021).
- [16] F. Schlawin, D. M. Kennes, and M. A. Sentef, Cavity quantum materials, *Appl. Phys. Rev.* **9**, 011312 (2022).
- [17] F. P. M. Méndez-Córdoba, J. J. Mendoza-Arenas, F. J. Gómez-Ruiz, F. J. Rodríguez, C. Tejedor, and L. Quiroga, Rényi entropy singularities as signatures of topological criticality in coupled photon-fermion systems, *Phys. Rev. Res.* **2**, 043264 (2020).
- [18] Z. Bacciconi, G. M. Andolina, and C. Mora, Topological protection of majorana polaritons in a cavity, *Phys. Rev. B* **109**, 165434 (2024).
- [19] L. Xu, J. Bai, W. Feng, and X.-Q. Li, Dynamics simulation of braiding two majorana zero modes via a quantum dot, *Phys. Rev. B* **108**, 115411 (2023).
- [20] B. Pandey, S. Okamoto, and E. Dagotto, Unexpected results for the non-trivial fusion of majorana zero modes in interacting quantum-dot arrays (2023), [arXiv:2311.15079](https://arxiv.org/abs/2311.15079) [cond-mat.mes-hall].
- [21] C.-X. Liu, H. Pan, F. Setiawan, M. Wimmer, and J. D. Sau, Fusion protocol for majorana modes in coupled quantum dots, *Phys. Rev. B* **108**, 085437 (2023).
- [22] L. C. Contamin, M. R. Delbecq, B. Douçot, A. Cottet, and T. Kontos, Hybrid light-matter networks of majorana zero modes, *npj Quantum Inf.* **7**, 10.1038/s41534-021-00508-w (2021).
- [23] M. Trif and Y. Tserkovnyak, Resonantly tunable majorana polariton in a microwave cavity, *Phys. Rev. Lett.* **109**, 257002 (2012).
- [24] M. Trif and P. Simon, Braiding of majorana fermions in a cavity, *Phys. Rev. Lett.* **122**, 236803 (2019).
- [25] F. P. M. Méndez-Córdoba, F. J. Rodríguez, C. Tejedor, and L. Quiroga, From edge to bulk: Cavity-induced displacement of topological nonlocal qubits, *Phys. Rev. B* **107**, 125104 (2023).
- [26] S. De Liberato, Light-matter decoupling in the deep strong coupling regime: The breakdown of the purcell effect, *Phys. Rev. Lett.* **112**, 016401 (2014).
- [27] Y. Ashida, I. Atac, and E. Demler, Cavity quantum electrodynamics at arbitrary light-matter coupling strengths, *Phys. Rev. Lett.* **126**, 153603 (2021).
- [28] See the Supplemental Material at url will be inserted by publisher, for details of the calculations and derivations.
- [29] F. J. Gómez-Ruiz, J. J. Mendoza-Arenas, F. J. Rodríguez, C. Tejedor, and L. Quiroga, Universal two-time correlations, out-of-time-ordered correlators, and leggett-garg inequality vi-

- olation by edge majorana fermion qubits, *Phys. Rev. B* **97**, 235134 (2018).
- [30] I. Fuentes-Guridi, S. Bose, and V. Vedral, Proposal for measurement of harmonic oscillator berry phase in ion traps, *Phys. Rev. Lett.* **85**, 5018 (2000).
- [31] V. Lahtinen and J. K. Pachos, A Short Introduction to Topological Quantum Computation, *SciPost Phys.* **3**, 021 (2017).
- [32] J. D. Sau and S. D. Sarma, Capacitance-based fermion parity read-out and predicted rabi oscillations in a majorana nanowire (2024), arXiv:2406.18080 [cond-mat.mes-hall].
- [33] R. W. Bomantara and J. Gong, Simulation of non-abelian braiding in majorana time crystals, *Phys. Rev. Lett.* **120**, 230405 (2018).
- [34] X. X. Yijia Wu, Jie Liu, Recent progress on non-abelian anyons: from majorana zero modes to topological dirac fermionic modes, *Sci. China Phys. Mech. Astron.* **66**, 267004 (2023).
- [35] Y. Shen, N. C. Harris, S. Skirlo, M. Prabhu, T. Baehr-Jones, M. Hochberg, X. Sun, S. Zhao, H. Larochelle, D. Englund, and M. Soljagic, Deep learning with coherent nanophotonic circuits, *Nature Photonics* **11**, 441–446 (2017).
- [36] J. M. Arrazola, V. Bergholm, and *et al.* Bradler, Quantum circuits with many photons on a programmable nanophotonic chip, *Nature* **591**, 54–60 (2021).
- [37] A. K. Feofanov, V. A. Oboznov, V. V. Bol’ginov, J. Lisenfeld, S. Poletto, V. V. Ryazanov, A. N. Rossolenko, M. Khabipov, D. Balashov, A. B. Zorin, P. N. Dmitriev, V. P. Koshelets, and A. V. Ustinov, Implementation of superconductor/ferromagnet/superconductor π -shifters in superconducting digital and quantum circuits, *Nature Physics* **6**, 593–597 (2010).
- [38] A. A. Abdumalikov, Jr, J. M. Fink, K. Juliusson, M. Pechal, S. Berger, A. Wallraff, and S. Filipp, Experimental realization of non-abelian non-adiabatic geometric gates, *Nature* **496**, 482 (2013).
- [39] S. Berger, M. Pechal, S. Pugnetti, A. A. Abdumalikov, L. Steffen, A. Fedorov, A. Wallraff, and S. Filipp, Geometric phases in superconducting qubits beyond the two-level approximation, *Phys. Rev. B* **85**, 220502(R) (2012).
- [40] S. Chaturvedi, M. S. Sriram, and V. Srinivasan, Berry’s phase for coherent states, *Journal of Physics A: Mathematical and General* **20**, L1071 (1987).
- [41] S. Gasparinetti, S. Berger, A. A. Abdumalikov, M. Pechal, S. Filipp, and A. J. Wallraff, Measurement of a vacuum-induced geometric phase, *Science Advances* **2**, 10.1126/sciadv.1501732 (2016).
- [42] M. Ayyash, X. Xu, and M. Mariantoni, Resonant schrodinger cat states in circuit quantum electrodynamics, *Phys. Rev. A* **109**, 023703 (2024)

—Supplemental Material—
**Cavity Control of Topological Qubits:
 Fusion Rule, Anyon Braiding and Majorana-Schrödinger Cat States**

Luis Quiroga¹, Fernando J. Gómez-Ruiz², Ivan A. Bocanegra-Garay², Ferney J. Rodríguez¹, & Carlos Tejedor^{3,4}

¹*Departamento de Física, Universidad de los Andes, A.A. 4976, Bogotá D.C, Colombia*

²*Departamento de Física Teórica, Atómica y Óptica, Universidad de Valladolid, 47011 Valladolid, Spain*

³*Departamento de Física Teórica de la Materia Condensada, Universidad Autónoma de Madrid, Madrid 28049, Spain*

⁴*Condensed Matter Physics Center (IFIMAC), Universidad Autónoma de Madrid, Madrid 28049, Spain*

Contents

I.	Kitaev Chain Cavity System	1
II.	Bulk single site case	2
A.	Time-dependent fusion rule control	3
III.	Two bulk sites case	4
A.	Braiding protocol in a two-site cavity	6
	References	8

KITAEV CHAIN CAVITY SYSTEM

We consider a general radiation-matter framework consisting of a KC interacting with a single quantum radiation mode within a cavity, whose Hamiltonian reads as $\hat{H} = \hat{H}_{\text{KC}} + \hat{H}_C + \hat{H}_X$. We restrict ourselves to a specific open boundary MC system whose Hamiltonian can be written in terms of spinless fermions as ($\hbar = 1$):

$$\hat{H}_{\text{KC}} = -\frac{\mu}{2} \sum_{j=1}^N [2\hat{c}_j^\dagger \hat{c}_j - \hat{1}] - \Delta \sum_{j=1}^{N-1} [\hat{c}_j^\dagger \hat{c}_{j+1} + \hat{c}_{j+1}^\dagger \hat{c}_j - \hat{c}_j \hat{c}_{j+1} - \hat{c}_{j+1}^\dagger \hat{c}_j^\dagger]. \quad (\text{S1})$$

Here \hat{c}_j (\hat{c}_j^\dagger) is the annihilation (creation) operator of spinless fermions at site $j = 1, \dots, N$. The chemical potential is denoted by μ whereas the hopping amplitude between nearest-neighbor sites and the nearest-neighbor two-fermion pairing interaction are taken identically as Δ (we assume $\Delta \geq 0$ without loss of generality). Within this homogeneous regime (which we will keep throughout the paper), the MC features two phases: a topological and a trivial phase. In the former phase a Majorana zero energy mode (MZEM) emerge whenever $|\mu| < 2\Delta$ [S1].

The single mode microcavity radiation Hamiltonian takes the usual form $\hat{H}_C = \omega \hat{a}^\dagger \hat{a}$, where ω is the photon quantum energy. Finally, \hat{H}_X , corresponds to the KC-microcavity coupling terms which reads as,

$$\hat{H}_X = \frac{1}{\sqrt{n_{\text{Cav}}}} \sum_{j \in \text{Cav}} \lambda_j \hat{c}_j^\dagger \hat{c}_j (e^{-i\phi_j} \hat{a}^\dagger + e^{i\phi_j} \hat{a}), \quad (\text{S2})$$

where $\lambda_j e^{-i\phi_j}$ the complex valued coupling strength between the KC j -site and the cavity field, Cav is the set with the site indices interacting with the cavity.

For vanishing chemical potential the single chain Kitaev Hamiltonian, Eq.(S1), reduces to a diagonal form in terms of new non-local fermion operators \hat{d}_j and \hat{d}_j^\dagger corresponding to the bond linking physical sites j and $j + 1$ of the KC:

$$\hat{H}_{\text{KC}} = 2\Delta \sum_{j=1}^{N-1} \left[\hat{d}_j^\dagger \hat{d}_j - \frac{1}{2} \right] = i\Delta \sum_{j=1}^{N-1} \gamma_{j,2} \gamma_{j+1,1}, \quad (\text{S3})$$

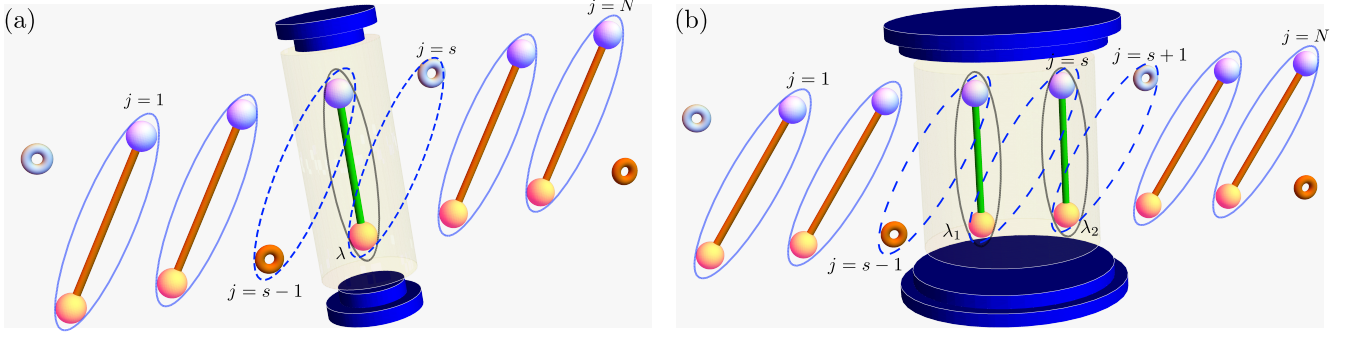


FIG. S1. **Bulk cases schematic representation of Kitaev chain cavity system.** In the topological phase, a Kitaev chain is schematically represented by colored balls and links. The balls represent Majorana fermions $\gamma_{j+1,1}$ and $\gamma_{j,2}$, with different colors indicating the localization of a free Majorana zero mode (MZM) as a torus. The cavity is depicted by two blue mirrors, which act as natural topological scissors. The KC-cavity interaction in the ultra-strong coupling (USC) regime allows for the formation of local Dirac fermions inside the cavity. Panel (a) corresponds to the single Kitaev chain (1CK) case, while panel (b) depicts the double Kitaev chain (2CK) case. The radiation-matter interaction is represented by λ_r , with $r = 1, 2$.

where:

$$\begin{aligned}\hat{d}_j &= \frac{i}{2} (\hat{c}_j^\dagger - \hat{c}_j + \hat{c}_{j+1}^\dagger + \hat{c}_{j+1}) = \frac{1}{2} (\hat{\gamma}_{j,2} + i\hat{\gamma}_{j+1,1}), \\ \hat{d}_j^\dagger &= \frac{i}{2} (\hat{c}_j^\dagger - \hat{c}_j - \hat{c}_{j+1}^\dagger - \hat{c}_{j+1}) = \frac{1}{2} (\hat{\gamma}_{j,2} - i\hat{\gamma}_{j+1,1}),\end{aligned}\quad (\text{S4})$$

or equivalently in terms of Majorana fermion (MF) operators $\hat{\gamma}_{j+1,1} = \hat{c}_{j+1}^\dagger + \hat{c}_{j+1} = i(\hat{d}_j^\dagger - \hat{d}_j)$ and $\hat{\gamma}_{j,2} = i(\hat{c}_j^\dagger - \hat{c}_j) = \hat{d}_j^\dagger + \hat{d}_j$ with $j = 1, \dots, N-1$. Obviously, d -fermions anti-commute $\{\hat{d}_j, \hat{d}_{j'}^\dagger\} = \delta_{j,j'}$. On the other hand, MF operators are Hermitian operators ($\hat{\gamma}_{i,v} = \hat{\gamma}_{i,v}^\dagger$) with $v = 1, 2$, they satisfy the property $(\hat{\gamma}_{i,v})^2 = 1$, and obey the modified anticommutation relations $\{\hat{\gamma}_{i,v}, \hat{\gamma}_{j,v'}\} = 2\delta_{i,j}\delta_{v,v'}$, with $i, j = 1, \dots, N$. From the definition of MF operators it is evident that for each spinless fermion on site j , two Majorana fermions are assigned to that site. It is important to note that the full chain length N is irrelevant for the vanishing chemical potential case.

BULK SINGLE SITE CASE

In this section, we consider the case when the chain-cavity coupling contribution at site $j = s$ of the KC in Eq. (S2) is the fermion number operator:

$$\begin{aligned}\hat{c}_s^\dagger \hat{c}_s &= \frac{1}{2} (1 + i\hat{\gamma}_{s,1}\hat{\gamma}_{s,2}), \\ &= \frac{1}{2} (1 + \hat{d}_{s-1}\hat{d}_s + \hat{d}_{s-1}\hat{d}_s^\dagger - \hat{d}_{s-1}^\dagger\hat{d}_s - \hat{d}_{s-1}^\dagger\hat{d}_s^\dagger).\end{aligned}\quad (\text{S5})$$

In panel (a) of Fig. S1, we schematically represent the bulk single-site case. Remarkably, for this coupling term the parity of the number of d -fermions is a constant of motion, i.e. a single photon can only produce changes on the d -fermion number by $0, \pm 2$. Since only two d -fermion operators (\hat{d}_{s-1} and \hat{d}_s) are included in the matter-radiation coupling term in Eq. (S5), just 4 matter (KC) states are involved in the full system quantum evolution. Therefore, the Kitaev even state sector is spanned by the basis set:

$$|-\rangle_z = |\text{vac}\rangle = |\circ\circ\rangle, \quad |+\rangle_z = \hat{d}_{s-1}^\dagger \hat{d}_s^\dagger |\circ\circ\rangle = |\bullet\bullet\rangle, \quad (\text{S6})$$

where $|\text{vac}\rangle = |\circ\circ\rangle$ represents the vacuum state, i.e. no d -fermion excitations or $|\circ\circ\rangle = 0$ for $j = s-1, s$. The full single-site cavity Hamiltonian converts to:

$$\begin{aligned}\hat{H}_1 &= 2\Delta \begin{pmatrix} -1 & 0 \\ 0 & 1 \end{pmatrix} + \omega \hat{a}^\dagger \hat{a} + \frac{\lambda}{2} (e^{-i\phi} \hat{a}^\dagger + e^{i\phi} \hat{a}) \begin{pmatrix} 1 & -1 \\ -1 & 1 \end{pmatrix}, \\ &= -2\Delta \hat{\sigma}_z + \omega \hat{a}^\dagger \hat{a} + \frac{\lambda}{2} (e^{-i\phi} \hat{a}^\dagger + e^{i\phi} \hat{a}) (1 - \hat{\sigma}_x),\end{aligned}\quad (\text{S7})$$

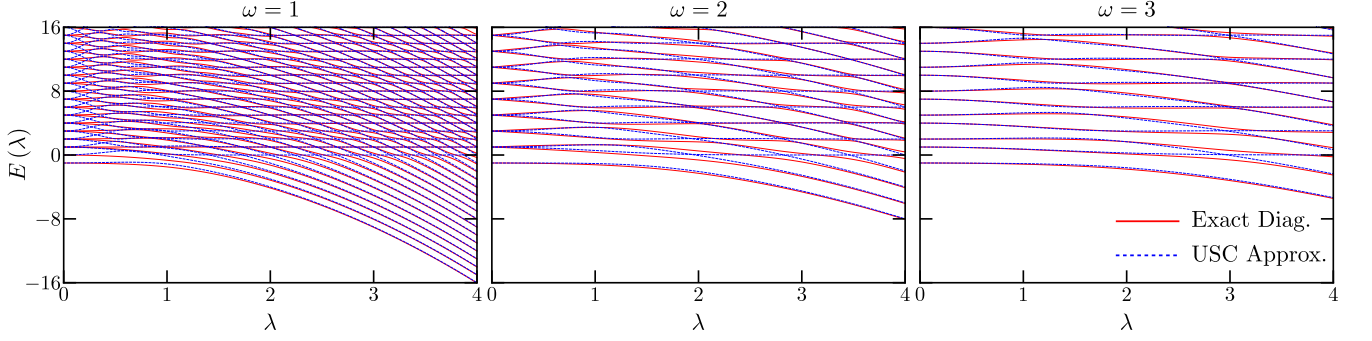


FIG. S2. **Energy Spectrum for the Bulk Single-Site Case.** Using Eq. (S7), we depict the exact numerical spectrum with red solid lines. We consider a controlled phase fixed at $\phi = 0$ and a qubit elemental energy $\Delta = 0.5$. Additionally, we validate the USC approximation given by Eq. (S8) for different values of the cavity frequency (from left to right $\omega = 1, 2, 3$). By directly substituting $n = 0, 1, 2, \dots$ and $\alpha = -\frac{\lambda}{\sqrt{2\omega}}e^{-i\phi}$ into Eq. (S8), we depict the USC approximation eigenenergies with dashed lines.

representing a **modified Rabi model** or driven Rabi model in the limit of static driving field.

Following a similar approach presented in Refs. [S2, S3], we obtain the approximate energy spectrum in the ultra-strong coupling regime (USC). Figures S2 depict the energy spectrum for different values of the cavity frequency from left to right $\omega/2\Delta = 1, 2, 3$ as a function of the light-matter coupling parameter. Continuous lines correspond to the exact numerical spectrum obtained by exact diagonalization of the Hamiltonian given by Eq. (S7) with a truncation in the Fock basis of 250 photons. On the other hand, dashed lines in Fig. S2 correspond to the USC approximation, where two-dimensional subspaces, spanned by basis sets $\{|-\rangle_x \otimes \hat{D}(\alpha)|n\rangle, |+\rangle_x \otimes |n'\rangle\}$, $n, n' = 0, 1, 2, \dots$, with $\alpha = -\frac{\lambda}{\sqrt{2\omega}}e^{-i\phi}$ and $\hat{D}(\alpha)$ the displacement operator, are separately diagonalized. For $n = n'$, the energies plotted as dashed lines in Fig. S2 turn out to be:

$$E_{n,\pm} = \frac{1}{2} \left[2n\omega - \frac{\lambda^2}{\omega} \pm \sqrt{\frac{\lambda^4}{\omega^2} + \Delta^2 e^{-4|\alpha|^2} L_n^2[4|\alpha|^2]} \right], \quad (\text{S8})$$

where $L_n(x)$ is a Laguerre polynomial.

In the weak-coupling regime ($\lambda < \omega \sim \Delta$) matter states given by Eq. (S6) are suited best for exploring the dynamics controlled by \hat{H}_1 . However, in the USC regime ($\lambda > \omega \sim \Delta$) a better adapted basis set is provided by occupation number states, $|n_{L,R}, n_c\rangle$, of a non-local fermion $f_{L,R} = \frac{1}{2}(\hat{\gamma}_L + i\hat{\gamma}_R)$ and a local fermion inside the cavity, $c_s = \frac{1}{2}(\hat{\gamma}_{s,1} + i\hat{\gamma}_{s,2})$. The basis transformation is:

$$\begin{aligned} |\circ\circ\rangle &= \frac{1}{\sqrt{2}} (|\circ_{L,R}, \circ_c\rangle - i|\bullet_{L,R}, \bullet_c\rangle), \\ |\bullet\bullet\rangle &= \frac{1}{\sqrt{2}} (|\circ_{L,R}, \circ_c\rangle + i|\bullet_{L,R}, \bullet_c\rangle). \end{aligned} \quad (\text{S9})$$

In this regime the ground state is simply expressed as $|GS\rangle \simeq -i|1_{L,R}, 1_c\rangle \otimes |\alpha\rangle$ with $\alpha = -\frac{\lambda}{\sqrt{2\omega}}e^{-i\phi}$.

Time-dependent fusion rule control

In the main text, we propose a fusion rule protocol in a KC-cavity system. In this subsection, we present the numerical strategies employed to obtain the time-dependent results for it. We consider a time-dependent light and matter coupling given by a linear pulse $\lambda = t/t_a$, where the annealing time t_a controls the velocity of the interaction. At $t = 0$, the cavity is uncoupled from the Kitaev chain and the initial state is the ground state of the Hamiltonian given by Eq. (S7) at $\lambda = 0$. By turning on the pulse, both systems begin to interact with a controlled annealing time t_a . We numerically obtain the state $|\psi(t)\rangle$ at time t by solving the time-dependent Schrödinger equation. We drive the system from the weak coupling regime to the ultra-strong coupling regime by manipulating the total evolution time t_f . As proposed in the main text, we calculate the fermion correlation given by

$$\begin{aligned} P(s-1, s+1)(t_f) &= i\langle \psi(t_f) | \gamma_{s-1,2} \gamma_{s+1,1} | \psi(t_f) \rangle, \\ &= -\langle \psi(t_f) | \hat{\sigma}_x | \psi(t_f) \rangle. \end{aligned} \quad (\text{S10})$$

The correlation $P(s-1, s+1)$ becomes a fingerprint of the fermion fusion rule. In Figure S3, we depict the behavior of this correlation as a function of the annealing time. Specifically, in Fig. S3(a) for the resonance case ($\Delta = 0.5$, $\omega = 2$), we evolve the system in the time window $t \in [0, 2t_a]$. At the final time $t_f = 2t_a$, we evaluate the correlation given by Eq. (S10). Following a similar procedure, in Fig. S3(b) we evolve the system from $t = 0$ to $t = 4t_a$ by using in panel left $\omega = 1$ and right $\omega = 3$ respectively. At the final time $t_f = 4t_a$, the system is in the USC regime, and we obtain a perfect correlation equal to 1.

TWO BULK SITES CASE

In Figure S1(b), the cavity couples with 2 nearest-neighbor bulk physical sites (s and $s+1$ with $s = 2, \dots, N-2$, or equivalently 3 bulk bond fermion modes are involved) characterized by the Hamiltonian:

$$\begin{aligned} \hat{H}_2 = & 2\Delta \sum_{r=-1,0,1} \left[\hat{d}_{s+r}^\dagger \hat{d}_{s+r} - \frac{1}{2} \right] + \omega \hat{a}^\dagger \hat{a} \\ & + \frac{1}{2\sqrt{2}} \sum_{r=0,1} \lambda_{r+1} \left(1 + \hat{d}_{s+r-1} \hat{d}_{s+r} + \hat{d}_{s+r-1} \hat{d}_{s+r}^\dagger - \hat{d}_{s+r-1}^\dagger \hat{d}_{s+r} - \hat{d}_{s+r-1}^\dagger \hat{d}_{s+r}^\dagger \right) (e^{-i\phi_{r+1}} \hat{a}^\dagger + e^{i\phi_{r+1}} \hat{a}), \end{aligned} \quad (\text{S11})$$

where complex valued $\lambda_1 e^{-i\phi_1}$ ($\lambda_2 e^{-i\phi_2}$) denote the coupling strength at site s ($s+1$). The last Hamiltonian conserves the parity of the number of fermions, i.e. it can only produce changes on the fermion number by $0, \pm 2$. Given the fact that the non-interacting matter-field ground-state has zero d -fermions, jointly with zero photons, it is natural to confine this study to the even sector of the fermion Hilbert space. Thus, just 4 matter (KC) states are involved in the full system quantum evolution. A mapping of the matter states to a two-spin system is thus immediate. In the following we restrict ourselves to the even KC-sector. In a two-spin basis formed by eigenvectors of z -Pauli matrix components $\{|+, +\rangle_z, |+, -\rangle_z, |-, +\rangle_z, |-, -\rangle_z\}$, the KC-matter states are now associated to:

$$\begin{aligned} |-, -\rangle_z &= |\circ_{s-1}, \circ_s, \circ_{s+1}\rangle, & |-, +\rangle_z &= |\circ_{s-1}, \bullet_s, \bullet_{s+1}\rangle, \\ |+, -\rangle_z &= |\bullet_{s-1}, \bullet_s, \circ_{s+1}\rangle, & |+, +\rangle_z &= |\bullet_{s-1}, \circ_s, \bullet_{s+1}\rangle. \end{aligned} \quad (\text{S12})$$

The free KC term in the Hamiltonian acquires an Ising-type spin-spin coupling term, yielding finally to:

$$\hat{H}_2 = -\Delta(\hat{\sigma}_{z,1} + \hat{\sigma}_{z,2} + \hat{\sigma}_{z,1} \hat{\sigma}_{z,2}) + \omega \hat{a}^\dagger \hat{a} + \frac{1}{2\sqrt{2}} \lambda_1 (\hat{a}^\dagger + \hat{a}) (1 - \hat{\sigma}_{x,1}) + \frac{1}{2\sqrt{2}} \lambda_2 (e^{-i\phi} \hat{a}^\dagger + e^{i\phi} \hat{a}) (1 - \hat{\sigma}_{x,2}). \quad (\text{S13})$$

Where $\phi_1 = 0$ and arbitrary $\phi_2 = \phi$ have been imposed to Eq. (S11). Thus, original information about d -fermion and Majorana fermions is now encoded in a basis set of two-spin states. Notice that the Hamiltonian expressed by Eq. (S13) represents an **inhomogeneous two-spin Rabi model**.

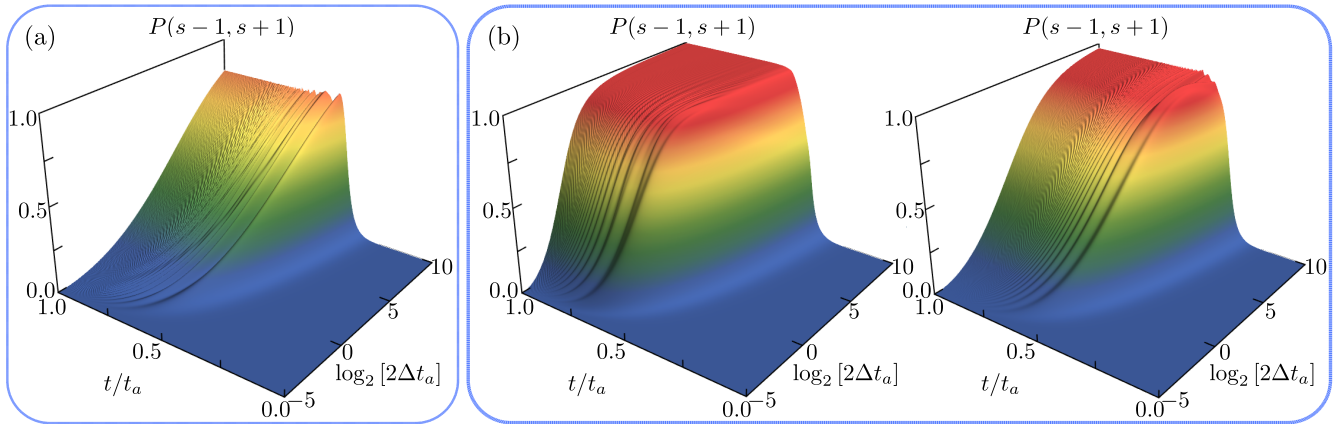


FIG. S3. **Time-Dependent Fusion Rule Control.** We consider a time-dependent light-matter interaction to validate the fusion rule using Eq. (S10). In panel (a), for the resonance case $\omega = 4\Delta$, we evolve the system in the time window $t \in [0, 2t_a]$. In panel (b), we consider the USC regime, evolving the system from 0 to $4t_a$. We use $\omega/2\Delta = 1$ and $\omega/2\Delta = 3$ in the left and right subpanels, respectively.

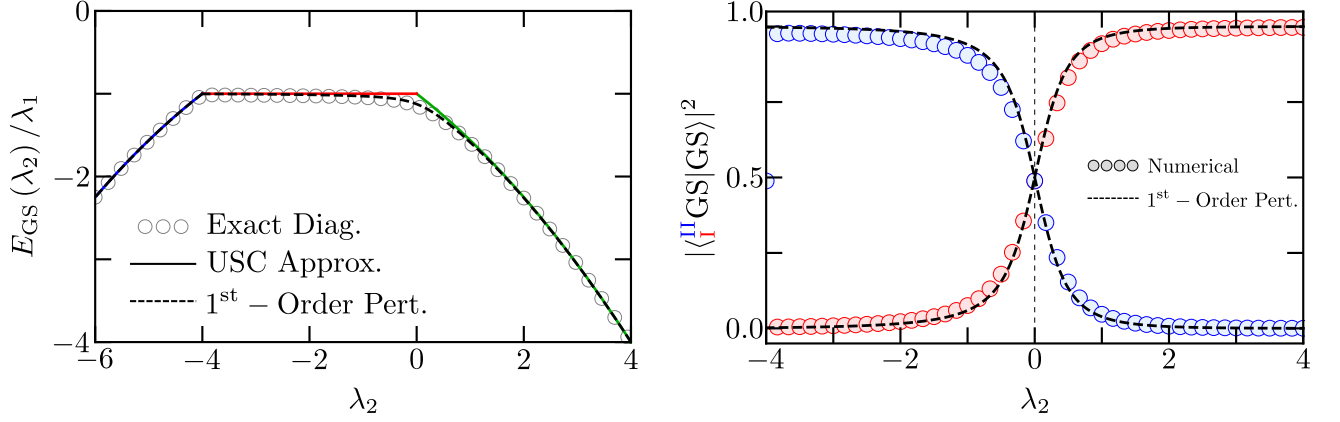


FIG. S4. **Ground state indicators for the two bulk sites case.** In the left panel, the symbols represent the ground state energy obtained by exact diagonalization of the Hamiltonian given by Eq. (S13) with $\lambda_1 = 4$ for the resonance case. The solid lines represent the USC approximation given by $E_{GS} = -\omega|\alpha|^2$, using α_{III} (Eq. (S17)) in the blue region, α_{II} (Eq. (S16)) in the red region, and α_I (Eq. (S16)) in the green region. The dashed black line corresponds to the exact results by first-order perturbation given by Eq. (S18). In the right panel, using the same parameters as the left panel, we contrast the numerical results (symbols) and the exact results by employing first-order perturbation theory (dashed lines) for the ground state fidelity. The blue/red symbols correspond to the numerical results obtained using Eq. (S15) and Eq. (S16), respectively. For the exact first-order perturbation results, we used Eq. (S19), with the corresponding angle given by Eq. (S20).

Similarly to the single site cavity case, in the weak-coupling regime matter states given by Eq. (S12) are suited best for exploring the dynamics controlled by \hat{H}_2 . Nevertheless, in the USC regime a better-adapted basis set is provided by occupation number states, $\{|n_{L,R}, n_{c_1}, n_{c_2}\rangle\}$, of a non-local fermion $f_{L,R} = \frac{1}{2}(\hat{\gamma}_L + i\hat{\gamma}_R)$ and two local fermions fully contained inside the cavity, $c_1 = \frac{1}{2}(\hat{\gamma}_{s,1} + i\hat{\gamma}_{s,2})$ and $c_2 = \frac{1}{2}(\hat{\gamma}_{s+1,1} + i\hat{\gamma}_{s+1,2})$. Now the basis transformation is:

$$\begin{aligned}
|-, -\rangle_z &= \frac{1}{2} \left[|o_{L,R}\rangle \otimes (|o_{c_1, o_{c_2}}\rangle + |\bullet_{c_1}, \bullet_{c_2}\rangle) - i|\bullet_{L,R}\rangle \otimes (|o_{c_1}, \bullet_{c_2}\rangle + |\bullet_{c_1}, o_{c_2}\rangle) \right], \\
|-, +\rangle_z &= \frac{1}{2} \left[|o_{L,R}\rangle \otimes (|o_{c_1}, o_{c_2}\rangle - |\bullet_{c_1}, \bullet_{c_2}\rangle) - i|\bullet_{L,R}\rangle \otimes (|o_{c_1}, \bullet_{c_2}\rangle - |\bullet_{c_1}, o_{c_2}\rangle) \right], \\
|+, -\rangle_z &= \frac{1}{2} \left[|o_{L,R}\rangle \otimes (|o_{c_1}, o_{c_2}\rangle - |\bullet_{c_1}, \bullet_{c_2}\rangle) + i|\bullet_{L,R}\rangle \otimes (|o_{c_1}, \bullet_{c_2}\rangle - |\bullet_{c_1}, o_{c_2}\rangle) \right], \\
|+, +\rangle_z &= \frac{1}{2} \left[|o_{L,R}\rangle \otimes (|o_{c_1}, o_{c_2}\rangle + |\bullet_{c_1}, \bullet_{c_2}\rangle) + i|\bullet_{L,R}\rangle \otimes (|o_{c_1}, \bullet_{c_2}\rangle + |\bullet_{c_1}, o_{c_2}\rangle) \right].
\end{aligned} \tag{S14}$$

In the USC regime, the ground state is simply expressed as $|GS\rangle \simeq |n_{L,R}\rangle \otimes |\Psi_{c_1, c_2, ph}\rangle$ where $|\Psi_{c_1, c_2, ph}\rangle$ is a composite state of fermions inside the cavity c_1 and c_2 , as well as cavity photons. Different regimes of relative values of λ_1 and λ_2 should be discriminated. Given $\lambda_1 > 0$, three different relative coupling sectors should be separately considered, as:

$$|GS\rangle_I = |o_{L,R}\rangle \otimes |\bullet_{c_1}, \bullet_{c_2}\rangle \otimes |\alpha_I\rangle, \quad \text{with } \alpha_I = -\frac{\lambda_1 + \lambda_2}{\sqrt{2}\omega}, \quad \text{for } \lambda_2 > 0, \tag{S15}$$

$$|GS\rangle_{II} = i|\bullet_{L,R}\rangle \otimes |o_{c_1}, \bullet_{c_2}\rangle \otimes |\alpha_{II}\rangle, \quad \text{with } \alpha_{II} = -\frac{\lambda_1}{\sqrt{2}\omega}, \quad \text{for } -\lambda_1 < \lambda_2 < 0, \tag{S16}$$

$$|GS\rangle_{III} = i|\bullet_{L,R}\rangle \otimes |\bullet_{c_1}, o_{c_2}\rangle \otimes |\alpha_{III}\rangle, \quad \text{with } \alpha_{III} = -\frac{\lambda_2}{\sqrt{2}\omega}, \quad \text{for } \lambda_2 < -\lambda_1. \tag{S17}$$

Numerical results for the ground state energy in each sector are depicted in Fig. S4, showing a good agreement with predicted USC analytical results, $E_{GS} = -|\alpha|^2\omega$. A crossing behavior is evident at $\lambda_2 = -\lambda_1$ due to the quasi-orthogonality of coherent states $|\alpha\rangle$ and $|\alpha\rangle$ for large values of λ , whereas an anti-crossing behavior takes place at $\lambda_2 = 0$. In the latter case, convenient approximate expressions can be found for both energies and ground state composition by considering the free fermion term in the Hamiltonian \hat{H}_2 , Eq. (S13), as a perturbation acting on the sub-space generated by states $\{|GS_+\rangle, |GS_-\rangle\}$. The ground state energy up to the first order in Δ is given by:

$$E_{GS} = -\frac{1}{2} \left[\omega (\alpha_I^2 + \alpha_{II}^2) + \sqrt{\omega^2 (\alpha_I^2 - \alpha_{II}^2)^2 + 4\Delta^2 |\langle \alpha_{II} | \alpha_I \rangle|^2} \right], \tag{S18}$$

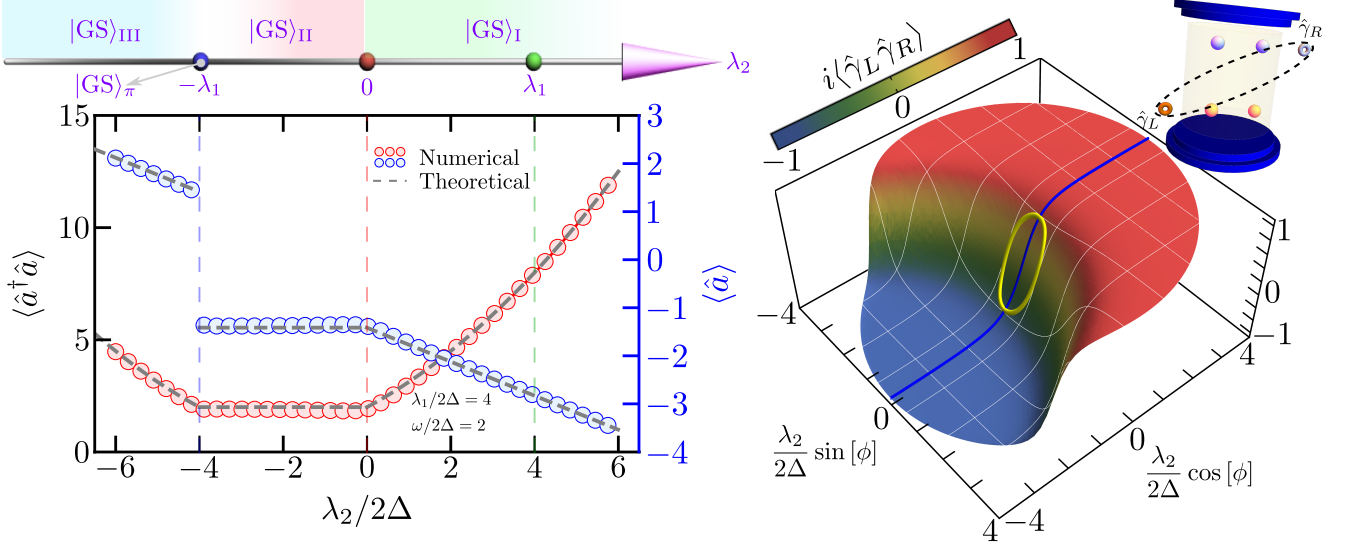


FIG. S5. **Parameter Regimes for the Ground State Structure and Braiding in a 2CK Setup.** In the left panel, we present a schematic representation of the ground state structure for 2KC as a function of λ_1 and λ_2 (see Eqs. (S15), (S16), and (S17)). Additionally, we validate the theoretical results for the ground state structure by numerically evaluating the expectation values of the operators $\hat{a}^\dagger \hat{a}$ and \hat{a} , and contrasting these numerical results with the theoretical predictions. In the right panel, we illustrate the landscape of parity between γ_L and γ_R . The solid blue line corresponds to the case where λ_2 is real and changes from positive to negative regimes. The closed yellow ring shows the evolution of the parity, demonstrating the perfect braiding between the Majorana fermions γ_L and γ_R , but now, in contrast to the main text, we used both outside MFs.

while the ground state in the transition regime becomes expressed as the superposition:

$$|\text{GS}\rangle = -\sin\left(\frac{\theta}{2}\right)|\text{GS}\rangle_{\text{I}} + \cos\left(\frac{\theta}{2}\right)|\text{GS}\rangle_{\text{II}}, \quad (\text{S19})$$

where

$$\tan(\theta) = -\frac{4\omega\Delta}{\lambda_2(\lambda_2 + 2\lambda_1)} e^{-\frac{\lambda_2^2}{4\omega^2}}. \quad (\text{S20})$$

Thus, it is evident that varying the coupling strength λ_2 of one physical site with the cavity and crossing the point $\lambda_2 = 0$, a cavity allowed *flip-flop effect* between the topological fermion state $|n_{L,R}\rangle$ and the local fermion $|n_{c1}\rangle$ is attained.

The point $\lambda_1 = \lambda_2 = \lambda$ and $\phi = \pi$ in Eq.(S13) deserves special attention because the system's ground state is not a separable matter-light state anymore. Instead, it can be expressed as a linear combination of local fermion qubits with photon Schrödinger cat states:

$$|\text{GS}\rangle_\pi \simeq |\bullet_{L,R}\rangle \otimes \left[(|o_{c1}, \bullet_{c2}\rangle + |\bullet_{c1}, o_{c2}\rangle) \otimes (|\alpha\rangle + |-\alpha\rangle) + (|o_{c1}, \bullet_{c2}\rangle - |\bullet_{c1}, o_{c2}\rangle) \otimes (|\alpha\rangle - |-\alpha\rangle) \right]. \quad (\text{S21})$$

with $\alpha = -\frac{\lambda}{\sqrt{2\omega}}$.

Braiding protocol in a two-site cavity

Consider a 2CK acting on chain sites $j = s$ (coupling strength $\lambda_1 e^{i\phi_1}$) and $j = s + 1$ (coupling strength $\lambda_2 e^{i\phi_2}$), governed by H_2 in Eq. (S13). Let us start by fixing $\lambda_1 > 0$ in the USC regime and $\phi_1 = 0$, without any loss of generality, while λ_2 and ϕ_2 can be tunable. The MF just to the left of the cavity, i.e. $\hat{\gamma}_L = \hat{\gamma}_{s-1,2}$, always behaves as a free MZM [S4] while the MF $\hat{\gamma}_R = \hat{\gamma}_{s+1,1}$ acquires the MZM condition only in the $\lambda_2 \rightarrow 0$ regime. We will be focusing on the braiding process between these two MFs, $\hat{\gamma}_L$ and $\hat{\gamma}_R$.

For that goal a better-adapted basis is provided by the set of occupation number states, $\{|n_{L,R}, n_c, n_{s+1}\rangle\}$, of a non-local fermion $f_{L,R} = \frac{1}{2}(\hat{\gamma}_L + i\hat{\gamma}_R)$, a local fermion fully contained inside the cavity, $\hat{c} = \frac{1}{2}(\hat{\gamma}_{s,1} + i\hat{\gamma}_{s,2})$ and the d -fermion \hat{d}_{s+1} . The basis transformation is:

$$|-, -\rangle_z = \frac{1}{\sqrt{2}} \left[|{}^{\circ}{}_{L,R}, {}^{\circ}{}_{c}\rangle - i|{}^{\bullet}{}_{L,R}, {}^{\bullet}{}_{c}\rangle \right] \otimes |{}^{\circ}{}_{s+1}\rangle, \quad |-, +\rangle_z = \frac{i}{\sqrt{2}} \left[|{}^{\circ}{}_{L,R}, {}^{\bullet}{}_{c}\rangle - i|{}^{\bullet}{}_{L,R}, {}^{\circ}{}_{c}\rangle \right] \otimes |{}^{\bullet}{}_{s+1}\rangle, \quad (\text{S22})$$

$$|+, -\rangle_z = \frac{1}{\sqrt{2}} \left[|{}^{\circ}{}_{L,R}, {}^{\circ}{}_{c}\rangle + i|{}^{\bullet}{}_{L,R}, {}^{\bullet}{}_{c}\rangle \right] \otimes |{}^{\circ}{}_{s+1}\rangle, \quad |+, +\rangle_z = -\frac{i}{\sqrt{2}} \left[|{}^{\circ}{}_{L,R}, {}^{\bullet}{}_{c}\rangle + i|{}^{\bullet}{}_{L,R}, {}^{\circ}{}_{c}\rangle \right] \otimes |{}^{\bullet}{}_{s+1}\rangle. \quad (\text{S23})$$

The USC composite ground state can also be written in this new basis as:

$$|\text{GS}_{\pm}\rangle = \begin{cases} -i|\Psi_+\rangle \otimes |\alpha_+\rangle, & \text{for } \phi_2 = 0, \\ +i|\Psi_-\rangle \otimes |\alpha_-\rangle, & \text{for } \phi_2 = \pi. \end{cases} \quad (\text{S24})$$

Where $|\Psi_{\pm}\rangle = \frac{1}{\sqrt{2}}(|{}^{\bullet}{}_{L,R}, {}^{\bullet}{}_{c}, {}^{\circ}{}_{s+1}\rangle \pm |{}^{\circ}{}_{L,R}, {}^{\bullet}{}_{c}, {}^{\bullet}{}_{s+1}\rangle)$, $\alpha_+ = -\frac{\lambda_1 + \lambda_2}{\sqrt{2\omega}}$ and $\alpha_- = -\frac{\lambda_1}{\sqrt{2\omega}}$ regardless the value of $\lambda_2 \leq \lambda_1$. In the 1CK limit, i.e. $\lambda_2 \rightarrow 0$, the system's ground state turns out to be

$$\begin{aligned} |\text{GS}\rangle &\simeq \frac{1}{\sqrt{2}} (|\text{GS}_+\rangle - |\text{GS}_-\rangle), \\ &= |{}^{\bullet}{}_{L,R}, {}^{\bullet}{}_{c}, {}^{\circ}{}_{s+1}\rangle \otimes |\alpha\rangle, \end{aligned} \quad (\text{S25})$$

with $\alpha = -\frac{\lambda_1}{\sqrt{2\omega}}$. The braiding or exchange process between $\hat{\gamma}_L$ and $\hat{\gamma}_R$ MFs, as described by the operator $\hat{U}_B^{(L,R)} = e^{\frac{\pi}{4}\hat{\gamma}_L\hat{\gamma}_R} = \frac{1}{\sqrt{2}}(1 + \hat{\gamma}_L\hat{\gamma}_R)$ (performing the exchange transformations $\hat{\gamma}_L \rightarrow \hat{\gamma}_R$ and $\hat{\gamma}_R \rightarrow -\hat{\gamma}_L$), when acting on the ground state produces the result $\hat{U}_B^{(L,R)}|\text{GS}\rangle = e^{-i\frac{\pi}{4}}|\text{GS}\rangle$. Our goal is to reach an identical phase transformation of the ground state after an appropriate adiabatic cyclic evolution of the coherent state $|\alpha\rangle$ by cycling the complex coupling strength $\lambda_2 e^{i\phi_2}$.

Now, we examine the possibility of reaching the same $e^{-i\frac{\pi}{4}}$ on the GS by performing an adiabatic cyclic evolution of the coherent cavity field (Berry phase). The ground state (GS) adiabatic evolution is fully contained in the two-dimensional sub-space spanned by the states $\{|\text{GS}_+\rangle, |\text{GS}_-\rangle\}$, as previously assured. Thus, the effective Hamiltonian matrix in that sub-space becomes:

$$\hat{H}_2 = \begin{pmatrix} -\omega|\alpha_+|^2 & \Delta\langle\alpha_-|\alpha_+\rangle \\ \Delta\langle\alpha_+|\alpha_-\rangle & -\omega|\alpha_-|^2 \end{pmatrix}. \quad (\text{S26})$$

With $\alpha_+ = -\frac{\lambda_1 + \lambda_2 e^{i\phi_2}}{\sqrt{2\omega}}$ and $\alpha_- = -\frac{\lambda_1}{\sqrt{2\omega}}$. We perform a cyclic evolution of the GS by fixing a $\lambda_2 > 0$ value while varying the phase $\phi_2 = \phi$ of the coupling strength, $0 \leq \phi \leq 2\pi$. Thus, for the GS we have

$$|\text{GS}(\phi)\rangle = C_+(\phi)|\text{GS}_+(\phi)\rangle + C_-(\phi)|\text{GS}_-(\phi)\rangle. \quad (\text{S27})$$

Notice that the state $|\text{GS}_-\rangle$ does not depend on the phase ϕ . We proceed with an analytical calculation of the Berry phase using Eq.(S26) and Eq.(S27). The Berry phase is given by:

$$\varphi_B = i \int_0^{2\pi} d\phi \langle \text{GS}(\phi) | \frac{\partial}{\partial \phi} | \text{GS}(\phi) \rangle. \quad (\text{S28})$$

Inserting Eq. (S27) into Eq. (S28) one gets

$$\varphi_B = \frac{\lambda_2}{4\omega^2} \int_0^{2\pi} d\phi \left(\lambda_2 + 2\lambda_1 \cos(\phi) \right) \left(1 + \frac{\lambda_2(\lambda_2 + 2\lambda_1 \cos(\phi))}{\sqrt{16\omega^2\Delta^2 e^{-\frac{\lambda_2^2}{2\omega^2}} + \lambda_2^2(\lambda_2 + 2\lambda_1 \cos(\phi))^2}} \right). \quad (\text{S29})$$

If $\Delta \ll \lambda_2$ the Berry phase $\Phi_B \rightarrow 2\pi(\frac{\lambda_2}{\sqrt{2\omega}})^2$, coinciding exactly with the Berry phase of a pure coherent state with $\alpha = -\frac{\lambda_2}{\sqrt{2\omega}}$ under an adiabatic cyclic evolution. A numerical evaluation of Eq.(S29) allows us to make a plot of λ_2 vs. λ_1 to get a Berry phase of just $\pi/4$, as shown in Fig. S5-a. As it is evident from that figure to reach the appropriate Berry phase the coupling strength with the right KC site $\lambda_2 \ll \lambda_1$, validating the ground state structure displayed by Eq.(S25). The parity $P_{L,R} = i\langle \hat{\gamma}_L \hat{\gamma}_R \rangle$,

between $\hat{\gamma}_L$ and $\hat{\gamma}_R$ Majorana fermions (MFs), is plotted in Fig. S5(b) as a function of $\lambda_2 e^{i\phi_2}$, for $0 \leq \lambda_2 \leq \lambda_1$ and $0 \leq \phi_2 \leq 2\pi$. $P_{L,R} \rightarrow -1$ for $\lambda_2 \approx 0$, in agreement with the ground state given by Eq. (S25). The solid line shows the corresponding results for varying real λ_2 values from the positive to the negative region. The closed curve depicts the evolution of $P_{L,R}$ at the λ_2 value producing the correct Berry phase of $\pi/4$, simulating the perfect braiding/exchange between $\hat{\gamma}_L$ and $\hat{\gamma}_R$ MFs.

[S1] A. Y. Kitaev, [Phys-Usp](#) **44**, 131-136 (2001)

[S2] D. Z. Rossatto, C. J. Villas-Bôas, M. Sanz, and E. Solano, [Phys. Rev. A](#) **96**, 013849 (2017)

[S3] Zi-Min Li and Murray T. Batchelor, [Phys. Rev. A](#) **104**, 033712 (2021)

[S4] F. P. M. Méndez-Córdoba, F. J. Rodríguez, C. Tejedor, and L. Quiroga, [Phys. Rev. B](#) **107**, 125104 (2023)